THE JOURNAL OF PHYSICAL CHEMISTRY C
A JOURNAL OF THE AMERICAN CHEMICAL SOCIETY

pubs.acs.org/JPCC

Article

Electrochemical Lithium Alloying Behavior of Guest-Free Type II Silicon Clathrates

Andrew Dopilka, Amanda Childs, Svilen Bobev, and Candace K. Chan*

Cite This: *J. Phys. Chem. C* 2021, 125, 19110−19118

Read Online

ACCESS | Metrics & More | Article Recommendations | Supporting Information

ABSTRACT: The guest-free type II Si clathrate (Si_{136}) is an open framework polymorph of Si that displays unique electrochemical reactions with Li. Li ions are first topotactically inserted into the vacant clathrate cages, followed by an alloying reaction that forms an amorphous lithium silicide phase. The alloying reaction voltage is higher than those seen in other Si electrodes, suggesting that there are structural differences in the formed amorphous phases. Synchrotron X-ray total scattering measurements and pair distribution function analysis are employed to characterize the amorphous phases formed after lithiation. The results show that the clathrate becomes completely amorphous at an earlier stage of lithiation when compared to diamond cubic Si, forming a phase with comparatively larger amounts of Si−Si bonding. The initial insertion of Li into the clathrate cages establishes important Li diffusion paths that kinetically enable the formation of an amorphous phase with lower Li content than typically seen in other silicon-based electrodes. After the initial crystalline-to-amorphous conversion reaction, lithiation takes place via solid-solution alloying. These results demonstrate how the topotactic insertion of Li into an alloying host can kinetically enable modified reaction pathways leading to more homogeneous lithiation throughout the electrode, which is beneficial for Li-ion battery applications.

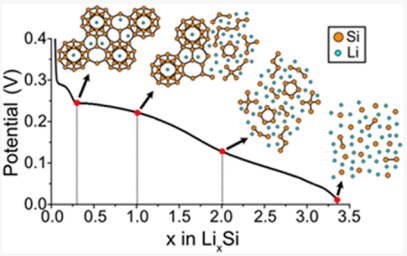

1. INTRODUCTION

Tetrel (Tt = Si, Ge, and Sn) clathrates are host−guest crystalline structures with a large compositional and structural space for tuning their properties.[1] Due to the interest in Tt-elements for Li-ion battery anodes, our group and others have been investigating Tetrel clathrates for applications as Li-ion battery anodes.[2−13] We have found that the cage structure and accompanying defects in clathrates result in significantly different electrochemical properties compared to the well-studied amorphous and diamond cubic elemental phases. For instance, we have shown that the Ba_8Ge_{43}, $Ba_8Al_{16}Ge_{30}$, and $Ba_8Ga_{15}Sn_{31}$ clathrates undergo solely amorphous phase transformations upon electrochemical reaction with Li, in contrast to the crystalline phase transformations typically observed in electrodes of the constituent elements (i.e., Ge, Al, Ga, and Sn).[13,14] Further, the amorphous phases formed after lithiation of the clathrates are retained in subsequent cycles and display promising electrochemical properties as alloying anodes for Li-ion batteries due to the solid-solution nature of the lithiation process and lower reaction voltage relative to those in elemental phases.

Given their open framework structure, we have also investigated the possibility of topotactic Li insertion into the cages of guest-free clathrates. We recently reported evidence of reversible Li insertion into nearly guest-free type II Si clathrates ($Na_{24-y}Si_{136}$, $y \sim 23$).[4] In the type II Si clathrate structure, Si dodecahedra (Si_{20}) and hexakaidecahedra (Si_{28}) are fused together into an open framework; the resultant cages may be filled with Na guest atoms (limiting composition of $Na_{24}Si_{136}$) or could be empty or nearly empty (limiting composition of $Na_{\sim 0}Si_{136}$).[15] Figure 1a shows a schematic of a Si_{20} (gray) and Si_{28} (blue) cage connected via a pentagonal face, and Figure 1b shows a polyhedral packing model of the clathrate II structure, illustrating the overall connectivity of the cages.

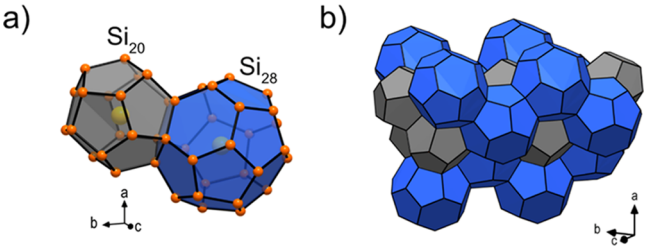

Figure 1. (a) Crystal model schematic of the dodecahedra (Si_{20}, gray) and the hexakaidecahedra (Si_{28}, blue) that comprise the type II Si clathrate structure with Na guest atoms in the cage centers. Si atoms are orange and Na atoms are yellow. (b) Polyhedral model of the type II clathrate $Na_{24-y}Si_{136}$.

Received: May 5, 2021
Revised: August 10, 2021
Published: August 30, 2021

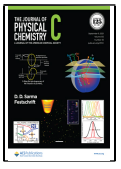

https://doi.org/10.1021/acs.jpcc.1c04020
J. Phys. Chem. C 2021, 125, 19110−19118

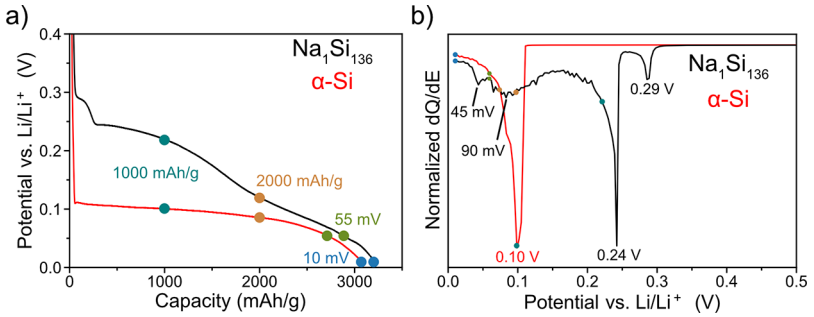

Figure 2. (a) Voltage profile and corresponding (b) normalized dQ/dE plot of the lithiation of Na_1Si_{136} and α-Si at 25 mA/g (~C/120) with a voltage cutoff of 10 mV vs Li/Li$^+$. The teal, orange, green, and blue dots represent the points at which cells were disassembled for *ex situ* measurements.

In our previous investigation of the lithiation properties of type II Si clathrates, we observed that topotactic Li insertion into the structure influenced the behavior of the Li alloying process that was observed after the addition of higher amounts of Li.[4] In nearly guest-free Si clathrates ($Na_{\sim 1}Si_{136}$), a voltage plateau at 0.26−0.30 V vs. Li/Li$^+$ was correlated to Li insertion into the vacant cages, resulting in a composition of $Li_{32}Si_{136}$. Immediately upon the incorporation of more Li, the lithiated clathrate phase ($Li_{32}Si_{136}$) then underwent a phase transformation attributed to the formation of an amorphous lithium silicide phase starting at 0.25 V.[2,4] On the other hand, when the Si clathrate cages were filled with Na guest atoms (i.e., as in $Na_{11}Si_{136}$ and $Na_{24}Si_{136}$), no voltage plateaus at either ~0.30 V (from Li insertion) or 0.25 V (from the conversion of crystalline $Li_{32}Si_{136}$ to amorphous lithium silicide) were observed. Rather, a single voltage plateau at 0.12−0.15 V was seen,[4,7] which is more similar to the lithiation process seen in diamond cubic Si (α-Si).[16,17] Because the process at 0.25 V was only observed if preceded by topotactic Li insertion into the clathrate (i.e., to form $Li_{32}Si_{136}$), we speculate that this Li insertion process kinetically enables the formation of an amorphous phase with a lower Li content than what is typically seen in the lithiation of α-Si. To investigate this phenomenon, herein, we use synchrotron X-ray total scattering measurements to obtain structure function and pair distribution function (PDF) plots to characterize the local and long-range structure of the amorphous intermediates formed during the electrochemical lithiation of the guest-free type II Si clathrate. By comparing the phases formed upon alloying the clathrate with Li to those seen when reacting diamond cubic Si (α-Si) to similar Li compositions, we aim to rationalize the structural origins of the potential-dependent phase transformations in the clathrate at degrees of lithiation that exceed the topotactic insertion process.

2. EXPERIMENTAL METHODS

The type II clathrate was synthesized via the thermal decomposition of Na_4Si_4 and prepared into electrodes as described in our previous work.[4] The electrodes were lithiated galvanostatically in half cells with lithium metal and then extracted for *ex situ* measurements. Synchrotron X-ray PDF measurements were conducted at Diamond Light Source (Didcot, United Kingdom) at the I15-I dedicated PDF beamline with λ = 0.161669 Å. The atomic PDF, $G(r)$ as defined by Farrow and Billinge et al.,[18] was generated from the total scattering data using PDFgetx3 within the xPDF suite software package.[19,20] Synchrotron XRD measurements were performed at the P02.1 powder diffraction beamline at PETRA III at the Deutsches Elektronen-Synchrotron (DESY) with λ = 0.20733 Å. More detailed descriptions of the synthesis, electrochemical and synchrotron measurements, and PDF analysis are provided in Supporting Information.

3. RESULTS

3.1. Electrochemical Lithiation. To investigate the structural origin of the alloying reaction in the type II clathrate electrodes observed beginning at 0.25 V versus Li/Li$^+$, *ex situ* synchrotron X-ray total scattering measurements were conducted after different amounts of Li were electrochemically inserted, with similar measurements performed on α-Si electrodes for comparison. The refinement of the as-prepared clathrate showed that the cages were nearly free of Na guest atoms, with a composition of $Na_{0.3(1)}Si_{136}$ and a lattice constant of 14.6484(8) Å (Figure S1, Table S1). Therefore, from here on, the clathrate sample will be referred to as Na_1Si_{136}. The voltage profiles and corresponding dQ/dE plots of the first lithiation of Na_1Si_{136} and α-Si are presented in Figure 2a,b, respectively, with teal, orange, green, and blue dots showing the points at which the samples were collected for *ex situ* total scattering measurements. The capacity and voltage corresponding to each of the colored dots for each sample are shown in Table S2.

The voltage profile and dQ/dE plot of lithiation of crystalline α-Si have already been described in detail in previous work[16,17] and are characterized by a voltage plateau and peak in the dQ/dE plot at 0.10 V versus Li/Li$^+$ corresponding to the two-phase conversion reaction between α-Si and an amorphous lithium silicide phase denoted as a-Li_xSi, where $x \sim 3.5$.[17] In the case of the Na_1Si_{136} electrode, a small voltage plateau and peak in the dQ/dE plot at 0.29 V are observed, which is attributed to the topotactic insertion of Li into the clathrate cages. This process and the underlying structural mechanism were described in detail in our previous work.[4] After the topotactic process, two-phase reaction is seen at 0.24 V versus Li/Li$^+$, which is assigned to the conversion of the lithiated clathrate to an amorphous phase.[2] As shown in Figure 2, this alloying reaction occurs at a higher voltage for the Na_1Si_{136} clathrate than for α-Si. It is also a higher voltage than that seen in Na-filled clathrates $Na_{24}Si_{136}$ (type II) and Na_8Si_{46} (type I), which also alloy with Li to form amorphous phases beginning at around 0.10−0.15 V versus Li/Li$^+$.[5,7] However, the alloying potential of Na_1Si_{136} is similar to the voltage seen in the lithiation of amorphous Si (0.25−0.30 V),[21−25] suggesting that these materials may be undergoing similar phase transformations (this will be discussed in further detail later). After the plateau at 0.24 V, the profile of Na_1Si_{136}

https://doi.org/10.1021/acs.jpcc.1c04020
J. Phys. Chem. C 2021, 125, 19110−19118

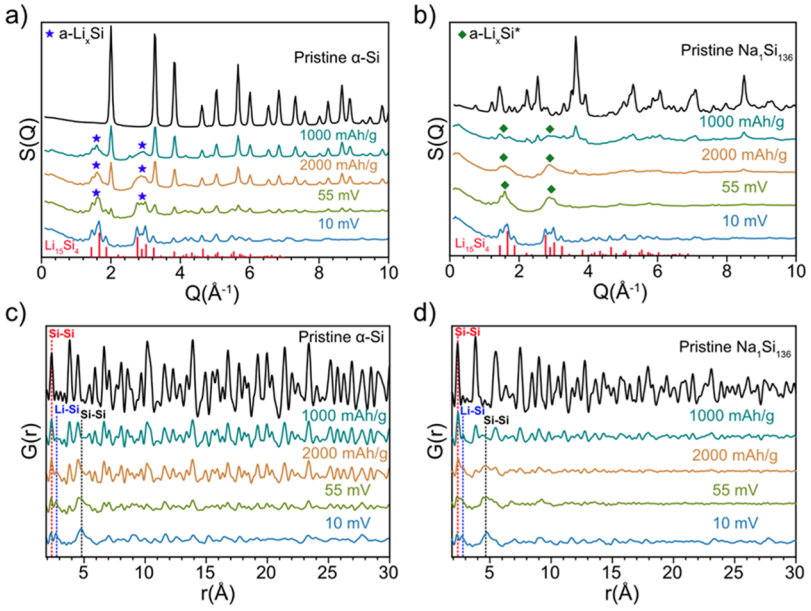

Figure 3. *Ex situ* (a,b) structure function and (c,d) PDF plots of the lithiation of (a,c) α-Si and (b,d) Na_1Si_{136} at the points marked in Figure 2.

becomes sloped until reaching the voltage cutoff at 10 mV. In the dQ/dE plot (Figure 2b), there are broad peaks centered at 90 and 45 mV. The broad peak at 90−100 mV is often seen in the dQ/dE plots of amorphous Si and is attributed to the breaking up of larger Si clusters in favor of smaller Si units such as Si−Si dumbbells and single atoms.[22,26] The peak at 45−50 mV is then attributed to the crystallization of the amorphous a-Li_xSi phase to crystalline $Li_{15}Si_4$.[22,27] Despite the identical lithiation capacity of 1000 mA h/g, we observe a large difference in the reaction potential between the α-Si and Si clathrate electrodes (~90 vs 220 mV), which implies that the lithium silicide amorphous phases, in either case, are structurally distinguishable. Therefore, analysis of structure function and PDF plots was conducted to identify the structural differences between these two different amorphous phases.

3.2. Structure Function and PDF Analysis. The structure function and PDF plots of α-Si and Na_1Si_{136} at the different points in the lithiation process indicated in Figure 2 are presented in Figure 3. The structure function plot is derived from the total scattering diffraction pattern and allows for the tentative identification of crystalline and amorphous phases present through comparison with calculated reference patterns. Figure 3a shows the structure function plots of the lithiation of α-Si, with the pristine (i.e., unlithiated) material showing reflections that match the calculated reference pattern of α-Si (Figure S2). At 1000 mA h/g (composition of $Li_{1.05}Si$), the reflections from α-Si are lower in intensity and broad peaks appear at around 1.8 and 2.4 Å^{-1} (marked by blue stars), indicating the growth of a lithiated amorphous Si phase (i.e., a-Li_xSi). Further lithiation to 2000 mA h/g ($Li_{2.10}Si$) shows a larger decrease in α-Si reflections and a growth in the broad peaks attributed to a-Li_xSi. At the 55 mV voltage cutoff (2650 mA h/g, $Li_{2.77}Si$), the pristine α-Si continues to be consumed in the reaction and the broad a-Li_xSi peaks begin to form separate peaks, likely related to the crystallization of $Li_{15}Si_4$. At 10 mV (3201 mA h/g, $Li_{3.35}Si$), the structure function plot matches that of $Li_{15}Si_4$ ($I\bar{4}3d$),[28] the phase formed upon full lithiation,[22] indicating that α-Si was completely consumed and a-Li_xSi was crystallized into $Li_{15}Si_4$. This behavior is consistent with previously reported *ex situ* and *in situ* XRD analysis of α-Si during lithiation,[17,22] where the two-phase reaction between α-Si and a-Li_xSi was correlated to the plateau at ~0.10 V and the crystallization of $Li_{15}Si_4$ from a-Li_xSi to the process at 50 mV.

For the guest-free type II clathrate (Na_1Si_{136}), the structure function plot of the pristine sample (Figure 3b) shows a good match with the calculated reference pattern of the type II Si clathrate (Figure S2). At a capacity of 1000 mA h/g ($Li_{1.05}Si$) and a potential of 0.22 V, the reflections corresponding to the pristine clathrate are greatly decreased in intensity and broad peaks appear around 1.8 and 2.4 Å^{-1} (marked by the green diamonds). These peaks, attributed to an amorphous lithium silicide phase (denoted a-Li_xSi* to differentiate from the a-Li_xSi phase that forms upon lithiation of α-Si), are broader than those seen in α-Si at 1000 mA h/g, which could be related to structural differences expected from the large observed difference in the potential as explained previously. At 2000 mA h/g ($Li_{2.10}Si$), the pristine clathrate has been almost completely consumed and the peaks associated with a-Li_xSi* increase in intensity. At this point in the lithiation process, the clathrate electrode appears to be almost completely amorphous, which is in contrast to the large fraction of α-Si still present at 2000 mA h/g for the lithiation of α-Si (Figure 3a). At 55 mV (2484 mA h/g, $Li_{2.60}Si$), all the pristine clathrate reflections have disappeared and only broad a-Li_xSi* peaks are present. At 10 mV (3118 mA h/g, $Li_{3.26}Si$), the broad peaks split into separate reflections that match those of $Li_{15}Si_4$, confirming that the process observed at 45 mV in the dQ/dE plot (Figure 2b) is related to the crystallization of $Li_{15}Si_4$. In summary, these structure function plots confirm the lithiation mechanism of α-Si and demonstrate that the Na_1Si_{136} clathrate structure, while like α-Si also undergoes a crystalline-to-amorphous conversion reaction, is completely consumed at an earlier stage in the lithiation process relative to that in α-Si. This results in the formation of a different type of amorphous lithiated intermediate phase than the one formed from α-Si, although both of these amorphous phases eventually crystallize into $Li_{15}Si_4$ at sufficiently low potentials.

https://doi.org/10.1021/acs.jpcc.1c04020
J. Phys. Chem. C 2021, 125, 19110−19118

To elucidate the local structural differences of the amorphous phases, the Fourier transform of the reduced structure functions was taken to generate the PDF plots.[18] Generally, the PDF results of the α-Si samples matched those reported in previous studies.[26] The PDF plot of pristine α-Si (Figure 3c) is well fit by a least-square refinement of the α-Si structure, confirming the purity of the pristine material (Figure S3a and Table S3). The first three correlations represent the first three coordination shells in α-Si, that is, from direct covalent Si−Si bonds (2.35 Å), second nearest neighbor (2.83 Å), and third nearest neighbor (4.50 Å) Si−Si distances (identified at 2.35, 3.8, and 4.5 Å by Key et al.[26]). After lithiation, the intensity of these α-Si correlations decreases, while there are notable changes at low r values (2−5 Å) that originate from the amorphous phase (a-Li_xSi) that is formed at the expense of α-Si as more Li is incorporated into the electrode. Three specific correlation distances are indicated with dotted lines in Figure 3c that correspond to direct Si−Si bonds (2.35 Å, red), Li−Si bonds (∼2.8 Å, blue), and first nonbonding Si−Si distances (∼4.7 Å, black). As Li is incorporated into the system, the silicon lattice is broken up and a decrease in the correlations related to Si−Si bonds is expected, while the new correlations from Li−Si bonds and nonbonding Si−Si correlations are expected to increase in intensity, as seen in the PDF taken from the electrode after lithiation to 1000 mA h/g. For α-Si lithiated to 10 mV, the PDF pattern was refined to crystalline $Li_{15}Si_4$ with a fairly good fit (R_w = 0.254) and a lattice parameter of 10.7126 Å (Figure S3b). The PDF also shows residual Si−Si correlations at 2.28 Å, which were attributed to Si−Si dimers in studies by Key et al.[26] and were incorporated into the refinement using the α-Si structure with a nanoparticle amplitude correction parameter of 4 Å. On the basis of the similarity of the peak positions between the new correlations that emerged in the PDF of the lithiated α-Si samples (at ∼2.8 Å from Li−Si and ∼4.7 Å from nonbonding Si−Si) with the low r correlations for $Li_{15}Si_4$ (as seen in the PDF of the 10 mV sample), we posit that these new correlations have a similar origin as those in $Li_{15}Si_4$. In the $Li_{15}Si_4$ structure,[28] the Si atoms are surrounded by Li atoms with a coordination number of 12 (Figure S4), so there are no direct Si−Si interactions. The PDF results confirm the reaction mechanism for lithiation of α-Si, whereby a lithiated amorphous phase forms in two-phase reaction at the expense of α-Si, with eventual crystallization to $Li_{15}Si_4$ at low potentials near the end of lithiation.

The PDFs for the lithiation of Na_1Si_{136} are shown in Figure 3d. The PDF of pristine Na_1Si_{136} fits well in the refinement with the type II Si structure model (Figure S3c). Notably, the first two Si−Si distances are similar in α-Si and Na_1Si_{136}; the third-nearest neighbor is 5.45 Å for the clathrate, while it is 4.50 Å for α-Si. This longer distance reflects the open cage structure of the type II clathrate. At a lithiation capacity of 1000 mA h/g, the correlations in the PDF significantly decrease in intensity, suggesting a decrease in the long-range order and that amorphization is occurring in the sample. As in the α-Si PDFs, correlations at 2.8 Å (Li−Si, blue) and 4.5−4.7 Å (Si−Si, black) begin to appear that correspond to Li−Si and nonbonded Si−Si correlations, respectively, while the correlation related to direct Si−Si bonds (2.35 Å, red) decreases. In the PDF of Na_1Si_{136} lithiated to 2000 mA h/g, the pristine clathrate appears to have been almost completely consumed in the reaction, consistent with the structure factor plot (Figure 3b). At 55 mV, the structure is highly disordered with broad peaks around 2.3−2.9 and 4.6−4.9 Å. At 10 mV, correlations at high r (20−30 Å) appear, evidence of the long-range order. As in α-Si, the amorphous phase formed during the initial lithiation of the clathrate crystallizes into $Li_{15}Si_4$ at the end of lithiation, which is supported by the PDF refinement (Figure S3d) and observation of $Li_{15}Si_4$ peaks in the structure function plot (Figure 3b). The PDF plots demonstrate that one of the major structural differences between the lithiation of α-Si and the type II Si clathrate is the Li composition at which the host structure is consumed during lithiation. The clathrate becomes completely consumed earlier in the lithiation process (by 2000 mA h/g or a composition of ∼$Li_{2.10}Si$), compared to 3201 mA h/g ($Li_{3.35}Si$) for α-Si. In other words, a smaller amount of Li reacting with the clathrate will cause complete amorphous phase formation compared to Li needed to fully consume α-Si.

To understand how the local structure of the lithiated amorphous phases derived from the two different starting materials differ, the PDFs of the lithiated electrodes were fit in the following manner. First, the crystalline contributions of the PDFs were fit to the structures of the pristine, unlithiated starting materials (α-Si and Na_1Si_{136}). On the basis that the lithiation process takes place via two-phase alloying reaction, the lithiated electrodes should consist of the unreacted crystalline starting phases and amorphous Li-containing phases; the difference curve of the refinement fit to the crystalline starting phase should therefore reveal the local structure information of the lithiated amorphous phase. These refinements are shown in Figure S5 (parameters in Tables S3 and S4), while the difference curves (with crystalline phases removed) are plotted and shown in Figure 4a,b. For the Na_1Si_{136} electrode lithiated to 10 and 55 mV, the actual PDF (rather than a difference curve) is shown in Figure 4b due to the absence of crystalline Na_1Si_{136} phases in these samples.

By subtracting away the correlations from the crystalline phases, the correlations corresponding to the amorphous phases are more evident in the difference curves. For example, the PDF pattern of α-Si after lithiation to 2000 mA h/g still contains a noticeable amount of α-Si, and the correlation around 4.75 Å attributed to the amorphous phase can be barely discerned (Figure 3c). However, the features originating from the amorphous phase are more clearly elucidated in the difference curves (Figure 4a). Due to the low scattering of lithium-rich phases to X-rays, some of the PDFs have noise that manifests as high-frequency ripples in the PDF plot. This is most evident in the difference curve of α-Si at 1000 mA h/g, likely due to the small amount of the amorphous phase present in the sample. Despite the noise, there are noticeable correlations centered at 2.35, 2.83, and 4.75 Å which, as described earlier, are attributed to Si−Si bonds, Li−Si bonds, and nonbonding Si−Si distances, respectively. The PDFs of the α-Si electrodes at the higher degrees of lithiation (2000 mA h/g, 55, 10 mV) look similar, suggesting a shared local structure. The main difference between the PDFs is the sharpness of the peaks corresponding to direct Si−Si (2.28−2.35 Å) and Li−Si (2.73−2.80 Å) bonds. The Si−Si and Li−Si correlations are merged in the sample lithiated to 2000 mA h/g, while the peaks begin to split as the potential goes from 55 to 10 mV. The broad peaks in the PDF at 2000 mA h/g are expected as this phase is completely amorphous, which results in a broadening of the PDF features due to the larger distribution of different Si and Li atomic environments. The subsequent sharpening of the peaks at lower potentials is consistent with

https://doi.org/10.1021/acs.jpcc.1c04020
J. Phys. Chem. C 2021, 125, 19110−19118

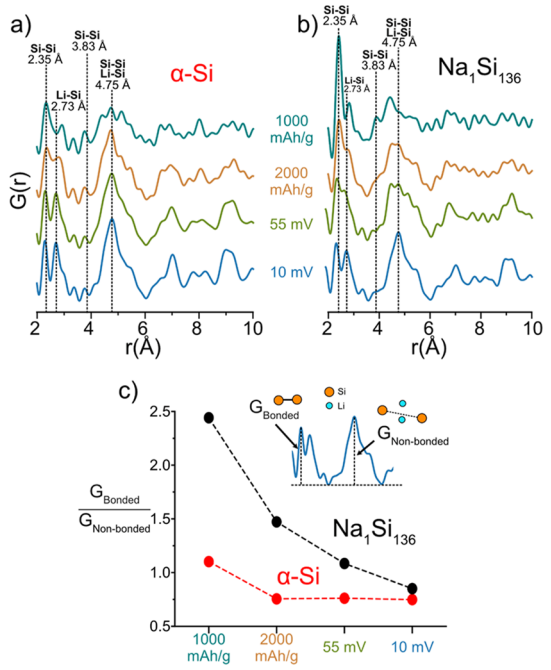

Figure 4. Difference curves of PDFs of lithiated (a) α-Si and (b) type II Na_1Si_{136} electrodes after fitting to crystalline α-Si or Na_1Si_{136}, respectively. The plots corresponding to the electrodes lithiated to 10 and 55 mV for Na_1Si_{136} are the actual PDF patterns (not difference curves). (c) Plot comparing the ratio of the intensity of the direct Si−Si correlations (G_{Bonded}) to the indirect Si−Si correlations ($G_{Nonbonded}$) at different stages of lithiation. The higher ratio gives a qualitative indication of a higher amount of Si−Si connectivity within the amorphous phase.

the crystallization of $Li_{15}Si_4$, which results in more defined Li−Si distances. Despite the changes in capacity and voltage, the local structure of the amorphous lithium silicide remains the same; this behavior is consistent with the two-phase reaction mechanism where, as Li enters the system, the lithium silicide phase grows at the expense of the unlithiated phase and the potential remains invariant.[29]

Another important factor is that the correlation related to direct Si−Si bonding at around 2.28−2.35 Å decreases in intensity compared to the correlation at 4.75 Å as the lithiation proceeds. The ratio of these correlations is a qualitative indication of the degree to which the Si matrix has been broken up by the incorporation of Li atoms. The larger the intensity of the peak at around 4.75 Å (which we call $G_{Nonbonded}$) relative to the one at 2.28−2.35 Å (G_{Bonded}) means that more Si−Si bonds are being broken to form isolated Si atoms, which is similar to the structure found in crystalline $Li_{15}Si_4$. This ratio of peak intensities is plotted and shown in Figure 4c, which shows the ratio of $G_{Bonded}/G_{Nonbonded}$ for the different samples. For α-Si (red curve), this ratio starts at 1.2 and then remains at 0.75 until the end of lithiation and crystallization of $Li_{15}Si_4$. The decrease in the ratio of $G_{Bonded}/G_{Nonbonded}$ as more Li is incorporated indicates that the amorphous lithiated phase that initially forms has a larger amount of Si clusters with retained Si−Si bonding compared to the amorphous lithiated phase found at higher degrees of lithiation (i.e., two distinct amorphous lithium silicide phases with different local structures). This interpretation is consistent with previous NMR studies showing two Li chemical shifts that correspond to Li next to Si clusters and Li surrounding isolated Si atoms at the beginning of lithiation of α-Si.[30] As the lithiation proceeds, the amount of Si clusters in the amorphous phase eventually decreases while isolated Si atoms increase, consistent with the lower amount of Si−Si bonds observed in the PDFs of α-Si with high Li content (2000 mA h/g, 55, 10 mV).

In contrast, the lithiated amorphous phases formed during lithiation of the clathrate are found to have an evolving local structure. From the difference curves shown in Figure 4b, the correlation at 2.35 Å, related to direct Si−Si bonds, has a much higher intensity relative to the correlations from 4−5 Å (related to next nearest neighbor Si−Si correlations) found in the PDF of the electrode lithiated to 1000 mA h/g. This indicates that a large amount of Si−Si connectivity from the original clathrate structure was retained in the amorphous phase. This is supported by the $G_{Bonded}/G_{Nonbonded}$ ratio shown in Figure 4c, showing a much higher ratio of connected Si to unconnected Si compared to α-Si lithiated at the same capacity (i.e., 2.5 vs 1.2 at 1000 mA h/g). This suggests that the different Si connectivity is one of the distinguishing features of the amorphous phases formed in α-Si versus clathrate electrodes. In addition, there is a notable peak at 3.83 Å in the PDFs of the clathrate samples that is related to the next-nearest neighbor correlations in a Si tetrahedron or Si pentagon, indicating that Si clusters of this size are still present in the amorphous phase.[26] The noise in the PDF of α-Si lithiated to 1000 mA h/g makes it difficult to distinguish whether or not a similar peak at 3.83 Å is present, but we believe that it is possible given the observation of Si clusters in the previous NMR studies.[26,30] The local structure of the amorphous phase formed after lithiation of the clathrate to 2000 mA h/g, the point at which the pristine phase has been almost completely consumed, shows a decrease in intensity in the correlations at 2.35 and 3.83 Å and an increase in intensity for the correlations around 4.75 Å, indicating that Si−Si bonds have been broken. Further lithiation to 55 mV shows a similar trend as that seen in α-Si where the $G_{Bonded}/G_{Nonbonded}$ ratio decreases, suggesting that lithiation proceeds through a continuous breaking of Si−Si bonds with the incorporation of more Li. At 10 mV, the local structure is similar to the one at 55 mV but with sharper and more defined correlations, consistent with the crystallization of $Li_{15}Si_4$.

To better understand the local structure of the lithiated clathrate at 1000 mA h/g and 2000 mA h/g, the two difference curves from the refinement are plotted with the simulated total and partial PDFs of $Li_{12}Si_7$ (Figure 5a), a crystalline phase comprising Si arranged in "stars" and pentagons (Figure 5b). Because the pristine clathrate structure contains Si atoms in both of these arrangements and because the composition of the electrode lithiated to 2000 mA h/g ($Li_{2.10}Si$) is similar to that of $Li_{12}Si_7$ ($Li_{1.71}Si$), we believe that this comparison could help to elucidate the local structure of the lithiated amorphous phase, a-Li_xSi*, present at this point of the lithiation process.

As shown in Figure 5a, the two shortest correlations in the total PDF of $Li_{12}Si_7$ correspond to direct Si−Si bonds and Li−Si bonds. Notably, the Li−Si correlations only contribute significantly to the total PDF at around 2.74 Å, while at higher distances, the Si−Si correlations dominate. The three correlations indicated with the dotted lines in the $Li_{12}Si_7$ total PDF (3.83, 4.25, and 4.62 Å) are identified and shown in Figure 5b, with the color of the bond matching the dotted line shown in Figure 5a. At 3.83 Å (cyan), there is a small peak in the calculated PDF pattern of $Li_{12}Si_7$ that corresponds to the

https://doi.org/10.1021/acs.jpcc.1c04020
J. Phys. Chem. C 2021, 125, 19110−19118

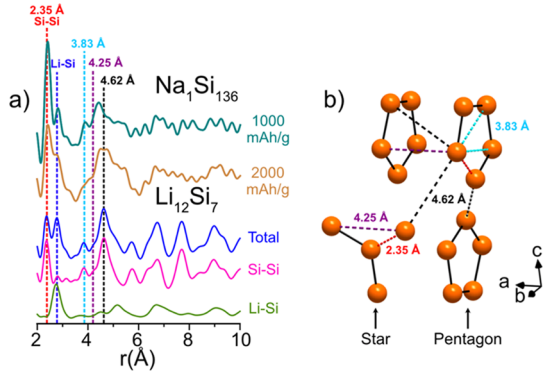

Figure 5. (a) Difference curves of PDFs of lithiated type II Na_1Si_{136} electrodes after fitting to crystalline Na_1Si_{136} and simulated total and partial PDF of $Li_{12}Si_7$. (b) Crystal structure model of $Li_{12}Si_7$ (from ref 31) displaying only the Si atoms. The dashed colored lines correspond to correlation distances in (a).

next-nearest neighbor distance in the Si pentagon. This correlation appears to be present in the PDFs of the clathrate lithiated to both 1000 and 2000 mA h/g, suggesting that similar Si−Si distances are present in the a-Li_xSi* amorphous phase. Next, there is a small correlation at around 4.25 Å (purple), which manifests as a shoulder to the larger peak at 4.62 Å (black). The former correlation corresponds to the Si−Si distance in $Li_{12}Si_7$ found between parallel Si pentagons as well as the edge of the Si_4 stars (purple). The latter corresponds to Si−Si correlations between the pentagon and star Si clusters (black). This distance (4.62 Å) matches the correlation seen in the 2000 mA h/g PDF but is larger than that observed in the 1000 mA h/g PDF (4.52 Å). Both of these correlations are shorter than the nonbonding Si−Si correlation at 4.70 Å for $Li_{15}Si_4$ (Figure S4a), suggesting that isolated Si atoms are not the major feature in the lithiated clathrate phases. This is consistent with the high $G_{Bonded}/G_{Nonbonded}$ ratio shown in Figure 4c. The correlations from ∼3.8 to 5.5 Å are broader than those in crystalline $Li_{12}Si_7$, which is expected for disordered amorphous phases. On the basis of the similar correlation distances in the amorphous phase seen in PDFs at 1000 and 2000 mA h/g as those in $Li_{12}Si_7$ as shown in Figure 5a and the higher $G_{Bonded}/G_{Nonbonded}$ ratio indicating more Si−Si bonding (Figure 4c), we expect that large Si clusters such as pentagons, stars, or other larger aggregates are present in the amorphous phase formed during the initial lithiation of the Si clathrate.

The PDF results show that the main structural differences in the amorphous phases formed upon lithiation of α-Si and the type II Si clathrate are related to (1) the Si−Si connectivity within the amorphous phase and (2) the amount of Li needed to fully amorphize the crystalline host. In the case of α-Si, an amorphous phase with high Li content (x in Li_xSi has been estimated to equal 3.5 based on an *in situ* XRD study[17]) is formed that contains a significant fraction of isolated Si atoms. In the type II Si clathrate, the amorphous phase forms with a lower Li content (around Li_2Si) and hence retains more Si−Si bonding. As lithiation proceeds, the degree of Si−Si connectivity continuously decreases until reaching a local structure similar to that in $Li_{15}Si_4$.

4. DISCUSSION

The electrochemical Li alloying mechanism in the type II Si clathrate can be summarized based on the presented results as follows (Figure 6). After topotactic Li insertion into the vacant cages (from 0.30 to 0.26 V), a flat plateau at 0.24 V is

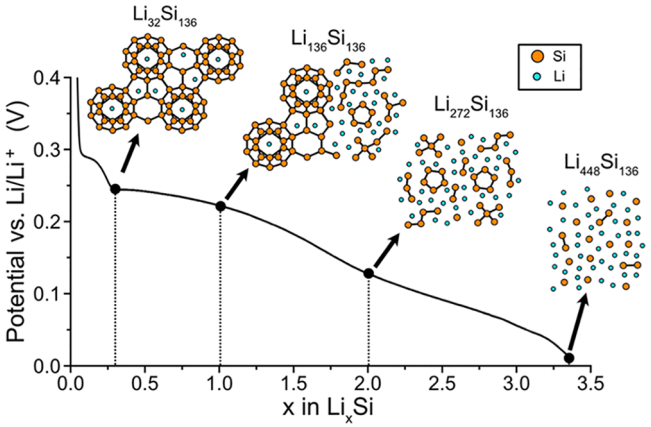

Figure 6. Proposed lithium alloying mechanism for the guest-free type II Si clathrate.

observed, which is followed by a sloped voltage profile until the voltage cutoff. The plateau at 0.24 V is assigned to the two-phase reaction between the lithiated clathrate ($Li_{32}Si_{136}$) and the amorphous a-Li_xSi* phase, where both phases are present until a composition of $Li_{1.05}Si$ (corresponding to a capacity of 1000 mA h/g). From the PDF analysis, the local structure of the amorphous a-Li_xSi* phase is proposed to consist of large Si clusters/chains with many direct Si−Si bonds. Considering that the original clathrate structure comprises Si atoms arranged in pentagons and hexagons, we believe that these Si clusters could be kinetically accessible at room temperature as only a few Si−Si bonds need to be broken to form them. This amorphous structure is notably different than one seen in α-Si at 1000 mA h/g (Figure 4a,c), which contains fewer Si−Si bonds. Because the chemical potential (and hence electrode potential) of the Li−Si phases is determined by the amount of Li in the phase and size of the Si clusters,[32−35] the number of Si−Si bonds is expected to correlate with the reaction voltage. We thus identify the large Si clusters in the amorphous clathrate phase as the origin of the higher reaction potential seen in the clathrate (0.22 V) compared to the α-Si (0.09 V) electrodes at the same lithiation capacity of 1000 mA h/g.

With the introduction of more Li, the pristine clathrate is almost completely consumed at a capacity of 2000 mA h/g (corresponding to a composition of $Li_{2.10}Si$). From the sloped voltage profile, it is expected that the lithiation process occurs as single-phase reaction where Li atoms distribute throughout the whole sample while continuously breaking Si−Si bonds, which results in a monotonic decrease in the potential. This is supported by Figure 4c, which shows a decrease in the $G_{Bonded}/G_{Nonbonded}$ peak ratio upon increasing lithiation. From the comparison of the PDF at a composition of $Li_{2.10}Si$ to the simulated PDF of crystalline $Li_{12}Si_7$ (Figure 5), we expect that similar Si clusters (i.e., pentagons and stars) could be present due to the analogous positioning of the Si−Si correlations.

As more Li enters the system to reach a composition of $Li_{3.30}Si$ and a potential of 10 mV, the amount of remaining Si−Si bonds decreases until the amorphous phase crystallizes to $Li_{15}Si_4$ with some residual Si−Si bonds remaining. The dQ/dE plot of the clathrate is characterized by a broad peak at 0.10 V versus Li/Li^+; a similar peak in the dQ/dE plot of the lithiation of amorphous Si has been attributed to the conversion of two

https://doi.org/10.1021/acs.jpcc.1c04020
J. Phys. Chem. C 2021, 125, 19110−19118

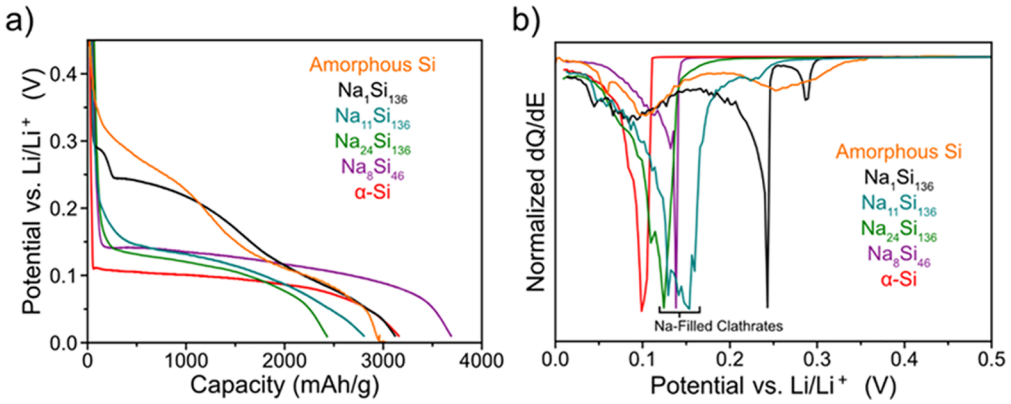

Figure 7. Comparison of the voltage profiles and dQ/dE plots of various reported Si structures. The data for Na_1Si_{136} and α-Si are from this work, that for $Na_{24}Si_{136}$ from ref 7, that for $Na_{11}Si_{136}$ from ref 4, that for Na_8Si_{46} from ref 5, and that for amorphous Si from ref 17.

distinct amorphous phases (a-$Li_{2.5}Si$ and a-$Li_{3.5}Si$).[26,36] After isolated Si atoms become the dominant feature, the a-Li_xSi* phase can then undergo the amorphous-to-crystalline phase transformation to form $Li_{15}Si_4$ due to the similar local structures.[37]

Based on these results, we liken the alloying behavior in the type II Si clathrate to be similar to that in amorphous Si. Numerous mechanisms have been proposed for the first cycle reaction between Li and amorphous Si, with certain analyses showing two-phase reactions between pristine amorphous Si and a distinct amorphous lithium silicide phase,[21,25,38] while others show single-phase behavior,[27,36,39] depending on the sample conditions and electrode parameters. Despite these opposing descriptions, it is generally agreed that lithium insertion into amorphous Si beyond the first cycle follows solid-solution behavior. An example dQ/dE plot of the lithiation of amorphous Si is reproduced and shown in Figure S6 and compared to that of the type II Si clathrate. Despite the different processes at high potentials (see Figure S6 for more details), the low potential processes associated with the Li alloying reactions are similar, suggesting that Li is able to spread across the Si matrix and continuously break Si−Si bonds via single-phase reaction in both materials.

From the comparison of the lithiation characteristics of Na_1Si_{136} to those of other clathrates, the effect of bulk Li diffusion throughout the whole Si matrix on the electrochemical profile becomes clear. This point is illustrated in Figure 7a,b, which compares the reported voltage and dQ/dE plots, respectively, for Na-filled Si clathrates from this and previous works,[5,7] along with those of amorphous Si[17] and α-Si. Upon lithiation, the Na-filled type II clathrates ($Na_{11}Si_{136}$ and $Na_{24}Si_{136}$) display voltage plateaus similar to that seen in α-Si and notably at lower potentials than the sloped voltage profiles from amorphous Si and nearly guest-free clathrate (Na_1Si_{136}). When the Si_{28} cages of the type II Si clathrate are filled with Na (as in the case of $Na_{11}Si_{136}$ and $Na_{24}Si_{136}$), Li has low diffusivity throughout the bulk as the Li migration barriers around the Na guest atoms are expected to be high.[4] Similarly, there is low Li diffusivity in α-Si.[40] This low Li diffusivity can explain the two-phase reaction mechanism seen in $Na_{11}Si_{136}$, $Na_{24}Si_{136}$, and α-Si, whereby lithiation occurs through a moving phase boundary between a lithiated and nonlithiated phase rather than homogenous lithiation through a solid solution. On the other hand, the topotactic insertion reaction of Li into Na_1Si_{136} allows for Li to spread throughout the Si matrix, forming $Li_{32}Si_{136}$ with Li sites in the Si_{28} cages throughout the electrode and establishes important diffusion paths that are maintained after amorphization occurs.[4] This allows the nearly guest-free type II Si clathrate to form an amorphous phase with a higher amount of retained Si−Si bonds than those found in the Na-filled clathrates, which is responsible for the higher voltage during the initial part of the lithiation process. Given that the clathrate host becomes amorphous at a composition with comparatively lower Li content, the reaction is then able to proceed through a single-phase reaction similar to that seen in the lithiation of amorphous Si.

Another interesting trend in the Na-filled clathrates ($Na_{11}Si_{136}$, $Na_{24}Si_{136}$, and Na_8Si_{46}) is that they all react at a higher voltage (around 0.12−0.15 V vs Li/Li$^+$) compared to α-Si (0.10 V) (Figure 7b). We speculate that this behavior could originate from the presence of the Na guest atoms within the Si framework, which provide extra electron density[41] that could aid in destabilizing the Si−Si bonds as Li is inserted and the amorphization process begins.[42] Because Si−Si bond breaking is expected to be the most kinetically difficult step of the reaction,[26] the presence of Na atoms could modify the local structure of the amorphous phase, which would change the reaction voltage. Future PDF studies would be insightful for confirming this speculation.

It is also interesting to note that the voltage characteristics of the type I clathrate, Na_8Si_{46},[5] are similar to those of the Na-filled type II clathrate ($Na_{24}Si_{136}$).[7] The type I clathrate structure has a different arrangement of polyhedral cages comprising six tetrakaidecahedra (Si_{24}) and two dodecahedra (Si_{20}) per unit cell. Though the arrangement of Si is slightly different in the type I and type II structures, the local structures are similar. Because both crystal structures become amorphous during electrochemical lithiation, the small differences in the initial crystalline structures are not expected to result in significant differences in the local structure after lithiation because the properties of the amorphous phases are dominated by local interactions. This is an important point as it suggests that the *composition* of the clathrate is more relevant for determining the electrochemical alloying behavior rather than the *structure* of the clathrate. In this case, we see that the alloying behavior in nearly Na-free clathrate is more similar to the solid-solution process seen in amorphous Si, whereas the Na-filled clathrates all display similar two-phase reactions. As explained earlier, this distinction likely has to do with the diffusivity of Li through the structure, with the presence of Na

https://doi.org/10.1021/acs.jpcc.1c04020
J. Phys. Chem. C 2021, 125, 19110−19118

guest atoms decreasing the Li diffusivity and inhibiting the single-phase reaction.

5. CONCLUSIONS

X-ray pair distribution analysis is used to investigate the amorphous alloying pathway of Na_1Si_{136} and compare it with that of diamond cubic structured α-Si. We find that after the initial insertion of Li into the empty cages, the clathrate goes through a two-phase reaction to form an amorphous phase with a high amount of Si−Si connectivity. Upon incorporation of more Li, the local structure of the amorphous phase changes via the continuous breaking of Si−Si bonds, resulting in a sloped voltage profile. Near the end of lithiation, broad peaks in the dQ/dE plot at 0.10 V and 50 mV are observed, which is similar to those seen in the lithiation of amorphous Si. The PDF measurements confirm that the observed feature at 45 mV corresponds to the amorphous-to-crystalline phase transformation to form $Li_{15}Si_4$, suggesting that the clathrate behaves similarly to conventional Si electrodes after the initial insertion and two-phase reaction.

The origin of the high-voltage two-phase reaction is attributed to the initial topotactic Li insertion process into the clathrate cages, which distributes Li throughout the Si matrix and forms crystalline $Li_{32}Si_{136}$. With the further addition of Li, an amorphous lithium silicide phase is formed but contains less Li than the amorphous phase formed during the lithiation of α-Si. This amorphous phase is then lithiated further through a single-phase reaction mechanism. These results not only elucidate the differences in lithiation properties of the type II Si clathrate compared to α-Si but also demonstrate how bulk Li insertion into the structure prior to alloying can lead to modified reaction paths by kinetically enabling the nucleation of amorphous phases with lower Li content.

■ ASSOCIATED CONTENT

Supporting Information

The Supporting Information is available free of charge at https://pubs.acs.org/doi/10.1021/acs.jpcc.1c04020.

Detailed experimental procedures for the synthesis of type II silicon clathrates, electrochemical measurements, sample preparation for synchrotron measurements, PDF analysis, powder XRD, Rietveld refinement parameters for the $Na_{0.3}Si_{136}$ clathrate, lithiation capacity and voltage of each clathrate and α-Si electrode, PDFgui refinement parameters for pristine α-Si and lithiated α-Si, PDFgui refinement parameters for the pristine Si clathrate and lithiated Si clathrate, Rietveld refinement plot of Na_1Si_{136}, structure function plots of α-Si and Na_1Si_{136}, PDF refinement plots of pristine α-Si and lithiated α-Si, PDF refinement plots of pristine Na_1Si_{136} and lithiated Na_1Si_{136}, and comparison of dQ/dE plots of amorphous Si and the type II Si clathrate (PDF)

■ AUTHOR INFORMATION

Corresponding Author

Candace K. Chan − *Materials Science and Engineering, School for Engineering of Matter, Transport and Energy, Arizona State University, Tempe, Arizona 85827, United States; Department of Heterogenous Catalysis, Max-Planck-Institut für Kohlenforschung, 45470 Mülheim an der Ruhr, Germany;* orcid.org/0000-0003-4329-4865; Phone: (480) 727-8614; Email: candace.chan@asu.edu

Authors

Andrew Dopilka − *Materials Science and Engineering, School for Engineering of Matter, Transport and Energy, Arizona State University, Tempe, Arizona 85827, United States;* orcid.org/0000-0003-3474-2187

Amanda Childs − *Department of Chemistry and Biochemistry, University of Delaware, Newark, Delaware 19716, United States*

Svilen Bobev − *Department of Chemistry and Biochemistry, University of Delaware, Newark, Delaware 19716, United States;* orcid.org/0000-0002-0780-4787

Complete contact information is available at: https://pubs.acs.org/10.1021/acs.jpcc.1c04020

Author Contributions

The manuscript was written through the contributions of all authors. A.D. performed the clathrate synthesis, prepared the electrodes, and performed the electrochemical measurements. A.D., A.C., and C.K.C. performed the sample preparation and conducted the synchrotron measurements. C.K.C. assisted with the electrochemical analysis and conceived the project with S.B. All authors have given approval to the final version of the manuscript.

Funding

Open access funded by Max Planck Society.

Notes

The authors declare no competing financial interest.

■ ACKNOWLEDGMENTS

This work was supported by funding from NSF from the awards DMR-1206795, DMR-1710017, DMR-1709813, DMR-2004514, and DMR-2004579. A.D. acknowledges support from ASU Fulton Schools of Engineering Dean's Fellowships. C.K.C. acknowledges support from the Max Planck Society and the Alexander von Humboldt Foundation for a Humboldt Research Fellowship. The authors also thank the Diamond Light Source (Didcot, UK) for access to beamline I15-1 (proposal no. CY22209) and T. Forrest and D. Keeble for assistance with PDF measurements. The authors also thank Deutsches Elektronen-Synchrotron (Hamburg, Germany) for access to beamline P02.1 (proposal no. I-20180707) and J. Tseng for assistance with synchrotron XRD measurements.

■ REFERENCES

(1) Dolyniuk, J.-A.; Owens-Baird, B.; Wang, J.; Zaikina, J. V.; Kovnir, K. Clathrate Thermoelectrics. *Mater. Sci. Eng., R* **2016**, *108*, 1−46.

(2) Langer, T.; Dupke, S.; Trill, H.; Passerini, S.; Eckert, H.; Pöttgen, R.; Winter, M. Electrochemical Lithiation of Silicon Clathrate-II. *J. Electrochem. Soc.* **2012**, *159*, A1318−A1322.

(3) Yang, J.; Tse, J. S. Silicon Clathrates as Anode Materials for Lithium Ion Batteries? *J. Mater. Chem. A* **2013**, *1*, 7782−7789.

(4) Dopilka, A.; Weller, J. M.; Ovchinnikov, A.; Childs, A.; Bobev, S.; Peng, X.; Chan, C. K. Structural Origin of Reversible Li Insertion in Guest-Free, Type-II Silicon Clathrates. *Adv. Energy Sustain. Res.* **2021**, *2*, 2000114.

(5) Dopilka, A.; Childs, A.; Bobev, S.; Chan, C. K. Solid-State Electrochemical Synthesis of Silicon Clathrates Using a Sodium-Sulfur Battery Inspired Approach. *J. Electrochem. Soc.* **2021**, *168*, 020516.

(6) Böhme, B.; Bonatto Minella, C.; Thoss, F.; Lindemann, I.; Rosenburg, M.; Pistidda, C.; Møller, K. T.; Jensen, T. R.; Giebeler, L.; Baitinger, M.; et al. B1-Mobilstor: Materials for Sustainable Energy

Storage Techniques - Lithium Containing Compounds for Hydrogen and Electrochemical Energy Storage. *Adv. Eng. Mater.* **2014**, *16*, 1189−1195.
(7) Wagner, N. A.; Raghavan, R.; Zhao, R.; Wei, Q.; Peng, X.; Chan, C. K. Electrochemical Cycling of Sodium-Filled Silicon Clathrate. *ChemElectroChem* **2014**, *1*, 347−353.
(8) Li, Y.; Raghavan, R.; Wagner, N. A.; Davidowski, S. K.; Baggetto, L.; Zhao, R.; Cheng, Q.; Yarger, J. L.; Veith, G. M.; Ellis-Terrell, C.; et al. Type I Clathrates as Novel Silicon Anodes: An Electrochemical and Structural Investigation. *Adv. Sci.* **2015**, *2*, 1500057.
(9) Peng, X.; Wei, Q.; Li, Y.; Chan, C. K. First-Principles Study of Lithiation of Type I Ba-Doped Silicon Clathrates. *J. Phys. Chem. C* **2015**, *119*, 28247−28257.
(10) Zhao, R.; Bobev, S.; Krishna, L.; Yang, T.; Weller, J. M.; Jing, H.; Chan, C. K. Anodes for Lithium-Ion Batteries Based on Type I Silicon Clathrate $Ba_8Al_{16}Si_{30}$ - Role of Processing on Surface Properties and Electrochemical Behavior. *ACS Appl. Mater. Interfaces* **2017**, *9*, 41246−41257.
(11) Dopilka, A.; Zhao, R.; Weller, J. M.; Bobev, S.; Peng, X.; Chan, C. K. Experimental and Computational Study of the Lithiation of $Ba_8Al_yGe_{46-y}$ Based Type I Germanium Clathrates. *ACS Appl. Mater. Interfaces* **2018**, *10*, 37981−37993.
(12) Dopilka, A.; Peng, X.; Chan, C. K. Ab Initio Investigation of Li and Na Migration in Guest-Free, Type I Clathrates. *J. Phys. Chem. C* **2019**, *123*, 22812−22822.
(13) Dopilka, A.; Childs, A.; Bobev, S.; Chan, C. K. Understanding the Amorphous Lithiation Pathway of the Type I Ba_8Ge_{43} Clathrate with Synchrotron X-Ray Characterization. *Chem. Mater.* **2020**, *32*, 9444−9457.
(14) Dopilka, A.; Childs, A.; Ovchinnikov, A.; Zhao, R.; Bobev, S.; Peng, X.; Chan, C. K. Structural and Electrochemical Properties of Type VIII $Ba_8Ga_{16-\delta}Sn_{30+\delta}$ Clathrate ($\delta \approx 1$) during Lithiation. *ACS Appl. Mater. Interfaces* **2021**, DOI: 10.1021/acsami.1c07240.
(15) Kasper, J. S.; Hagenmuller, P.; Pouchard, M.; Cros, C. Clathrate Structure of Silicon Na_8Si_{46} and Na_xSi_{136} (x < 11). *Science* **1965**, *150*, 1713−1714.
(16) Obrovac, M. N.; Krause, L. J. Reversible Cycling of Crystalline Silicon Powder. *J. Electrochem. Soc.* **2007**, *154*, A103−A108.
(17) Li, J.; Dahn, J. R. An In Situ X-Ray Diffraction Study of the Reaction of Li with Crystalline Si. *J. Electrochem. Soc.* **2007**, *154*, A156−A161.
(18) Farrow, C. L.; Billinge, S. J. L. Relationship between the Atomic Pair Distribution Function and Small-Angle Scattering: Implications for Modeling of Nanoparticles. *Acta Crystallogr., Sect. A: Found. Adv.* **2009**, *65*, 232−239.
(19) Juhás, P.; Davis, T.; Farrow, C. L.; Billinge, S. J. L. PDFgetX3: A Rapid and Highly Automatable Program for Processing Powder Diffraction Data into Total Scattering Pair Distribution Functions. *J. Appl. Crystallogr.* **2013**, *46*, 560−566.
(20) Yang, X.; Juhas, P.; Farrow, C. L.; Billinge, S. J. L. xPDFsuite: An End-to-End Software Solution for High Throughput Pair Distribution Function Transformation, Visualization and Analysis. https://arxiv.org/abs/1402.3163 (accessed Feb 23, 2015).
(21) Wang, J. W.; He, Y.; Fan, F.; Liu, X. H.; Xia, S.; Liu, Y.; Harris, C. T.; Li, H.; Huang, J. Y.; Mao, S. X.; et al. Two-Phase Electrochemical Lithiation in Amorphous Silicon. *Nano Lett.* **2013**, *13*, 709−715.
(22) Obrovac, M. N.; Christensen, L. Structural Changes in Silicon Anodes during Lithium Insertion/Extraction. *Electrochem. Solid-State Lett.* **2004**, *7*, A93−A96.
(23) Jung, H.; Park, M.; Yoon, Y. G.; Kim, G. B.; Joo, S. K. Amorphous Silicon Anode for Lithium-Ion Rechargeable Batteries. *J. Power Sources* **2003**, *115*, 346−351.
(24) Maranchi, J. P.; Hepp, A. F.; Kumta, P. N. High Capacity, Reversible Silicon Thin-Film Anodes for Lithium-Ion Batteries. *Electrochem. Solid-State Lett.* **2003**, *6*, A198−A201.
(25) Uxa, D.; Jerliu, B.; Hüger, E.; Dörrer, L.; Horisberger, M.; Stahn, J.; Schmidt, H. On the Lithiation Mechanism of Amorphous Silicon Electrodes in Li-Ion Batteries. *J. Phys. Chem. C* **2019**, *123*, 22027−22039.
(26) Key, B.; Morcrette, M.; Tarascon, J.-M.; Grey, C. P. Pair Distribution Function Analysis and Solid State NMR Studies of Silicon Electrodes for Lithium Ion Batteries: Understanding the (De)Lithiation Mechanisms. *J. Am. Chem. Soc.* **2011**, *133*, 503−512.
(27) Hatchard, T. D.; Dahn, J. R. In Situ XRD and Electrochemical Study of the Reaction of Lithium with Amorphous Silicon. *J. Electrochem. Soc.* **2004**, *151*, A838−A842.
(28) Zeilinger, M.; Baran, V.; van Wüllen, L.; Häussermann, U.; Fässler, T. F. Stabilizing the Phase $Li_{15}Si_4$ through Lithium-Aluminum Substitution in $Li_{15-x}Al_xSi_4$ (0.4 < x < 0.8) - Single Crystal X-Ray Structure Determination of $Li_{15}Si_4$ and $Li_{14.37}Al_{0.63}Si_4$. *Chem. Mater.* **2013**, *25*, 4113−4121.
(29) Huggins, R. A. *Advanced Batteries: Materials Science Aspects*; Springer Science & Business Media, 2008.
(30) Key, B.; Bhattacharyya, R.; Morcrette, M.; Seznéc, V.; Tarascon, J.-M.; Grey, C. P. Real-Time NMR Investigations of Structural Changes in Silicon Electrodes for Lithium-Ion Batteries. *J. Am. Chem. Soc.* **2009**, *131*, 9239−9249.
(31) Wu, H.; Hartman, M. R.; Udovic, T. J.; Rush, J. J.; Zhou, W.; Bowman, R. C.; Vajo, J. J. Structure of the Novel Ternary Hydrides Li_4Tt_2D (Tt = Si and Ge). *Acta Crystallogr., Sect. B: Struct. Sci.* **2007**, *63*, 63−68.
(32) Sivonxay, E.; Aykol, M.; Persson, K. A. The Lithiation Process and Li Diffusion in Amorphous SiO_2 and Si from First-Principles. *Electrochim. Acta* **2020**, *331*, 135344.
(33) Chou, C.-Y.; Kim, H.; Hwang, G. S. A Comparative First-Principles Study of the Structure, Energetics, and Properties of Li-M (M = Si, Ge, Sn) Alloys. *J. Phys. Chem. C* **2011**, *115*, 20018−20026.
(34) Chevrier, V. L.; Dahn, J. R. First Principles Model of Amorphous Silicon Lithiation. *J. Electrochem. Soc.* **2009**, *156*, A454−A458.
(35) Chevrier, V. L.; Dahn, J. R. First Principles Studies of Disordered Lithiated Silicon. *J. Electrochem. Soc.* **2010**, *157*, A392−A398.
(36) Li, J.; Smith, A.; Sanderson, R. J.; Hatchard, T. D.; Dunlap, R. A.; Dahn, J. R. In Situ ^{119}Sn Mössbauer Effect Study of the Reaction of Lithium with Si Using a Sn Probe. *J. Electrochem. Soc.* **2009**, *156*, A283−A288.
(37) Gu, M.; Wang, Z.; Connell, J. G.; Perea, D. E.; Lauhon, L. J.; Gao, F.; Wang, C. Electronic Origin for the Phase Transition from Amorphous Li_xSi to Crystalline $Li_{15}Si_4$. *ACS Nano* **2013**, *7*, 6303−6309.
(38) McDowell, M. T.; Lee, S. W.; Harris, J. T.; Korgel, B. A.; Wang, C.; Nix, W. D.; Cui, Y. In Situ TEM of Two-Phase Lithiation of Amorphous Silicon Nanospheres. *Nano Lett.* **2013**, *13*, 758−764.
(39) Wang, X.; Singh, S. S.; Ma, T.; Lv, C.; Chawla, N.; Jiang, H. Quantifying Electrochemical Reactions and Properties of Amorphous Silicon in a Conventional Lithium-Ion Battery Configuration. *Chem. Mater.* **2017**, *29*, 5831−5840.
(40) Hüger, E.; Dörrer, L.; Schmidt, H. Permeation, Solubility, Diffusion and Segregation of Lithium in Amorphous Silicon Layers. *Chem. Mater.* **2018**, *30*, 3254−3264.
(41) Tse, J. S.; Uehara, K.; Rousseau, R.; Ker, A.; Ratcliffe, C. I.; White, M. A.; MacKay, G. Structural Principles and Amorphouslike Thermal Conductivity of Na-Doped Si Clathrates. *Phys. Rev. Lett.* **2000**, *85*, 114−117.
(42) Zhao, K.; Wang, W. L.; Gregoire, J.; Pharr, M.; Suo, Z.; Vlassak, J. J.; Kaxiras, E. Lithium-Assisted Plastic Deformation of Silicon Electrodes in Lithium-Ion Batteries: A First-Principles Theoretical Study. *Nano Lett.* **2011**, *11*, 2962−2967.